Annals of Nuclear Medicine Vol. 13, No. 3, 199–203, 1999

Easy detection of tumor in oncologic whole-body PET by projection reconstruction images with maximum intensity projection algorithm

Takehiko FUJIWARA,*,** Masayasu MIYAKE,** Shoichi WATANUKI,**
Marco A. MEJIA,** Masatoshi ITOH** and Hiroshi FUKUDA*

*Department of Nuclear Medicine and Radiology, Institute of Development, Aging and Cancer, Tohoku University
**Cyclotron and Radioisotope Center, Tohoku University

Whole-body PET scanning for an oncology study produces a large number of transaxial images by data acquisition over multiple bed positions. The sagittal and coronal reformatted images are often used for better understanding of radioisotope distribution. We reduced the number of PET images by calculating projection images and evaluated the merit of additional data processing for the visualization and detection of tumors. After reconstructing whole-body ^{18}F-FDG PET images (6–8 bed positions) of eight cancer patients, antero-posterior and lateral projection images were calculated by the maximum intensity projection (MIP) algorithm, the standard deviation projection (SD) algorithm and the summed voxel projection (SUM) algorithm. The projection images were compared with 2D whole-body images for visualizing foci. The focal uptakes of various positions in original whole-body PET data (294–392 transaxial images) were visualized on only two MIP reformatted images when superimposition of hot spots did not occur. Even if one hot spot was superimposed over the other hot spot, we could recognize the existence of at least one focus and determine the true positions of the hot spots from corresponding transaxial images. The SD image was found inferior for showing a contrast of small foci to the corresponding MIP images in the neck, mediastinum and abdomen. The SUM image failed to visualize many metastatic lesions. MIP is a promising technique for the easy preliminary assessment of tumor distribution in oncologic whole-body PET study.

Key words: whole-body PET, 3D display, maximum intensity projection, cancer study, FDG

INTRODUCTION

WHOLE-BODY PET has become an important modality to evaluate oncology patients. It has been used as a non-invasive method for tumor staging, management of on-going therapy and even for cancer screening.[1–4] The extended axial field-of-view of the PET scanner obtained by data acquisition over multiple bed positions provided hundreds of transaxial images in the whole-body PET protocol. Since the easy detection of positive foci in a large number of PET images is an important clue to daily cancer diagnosis, the sagittal and coronal reformatted images are often used for assessment of radioisotope distribution by reducing the number of images. However, to overview the whole body images, sequential observation of 30–40 reformatted images and mental reconstruction of 3D relationship are still required.

To glance over all the information in 3D volume image data, projection algorithms are commonly used. The surface rendering technique has been applied to visualize the 3D data set of a brain PET image.[5] This procedure has limitation when applied to whole-body PET images because only individual predefined tissue surfaces can be visualized, and it is difficult to visualize the distribution of

Received November 2, 1998, revision accepted March 16, 1999.

For reprint contact: Takehiko Fujiwara, M.D., Ph.D., Department of Nuclear Medicine and Radiology, Institute of Development, Aging and Cancer, Tohoku University, Seiryo-cho 4–1, Aoba-ku, Sendai 980–8575, JAPAN.
E-mail: fujiwara@idac.tohoku.ac.jp

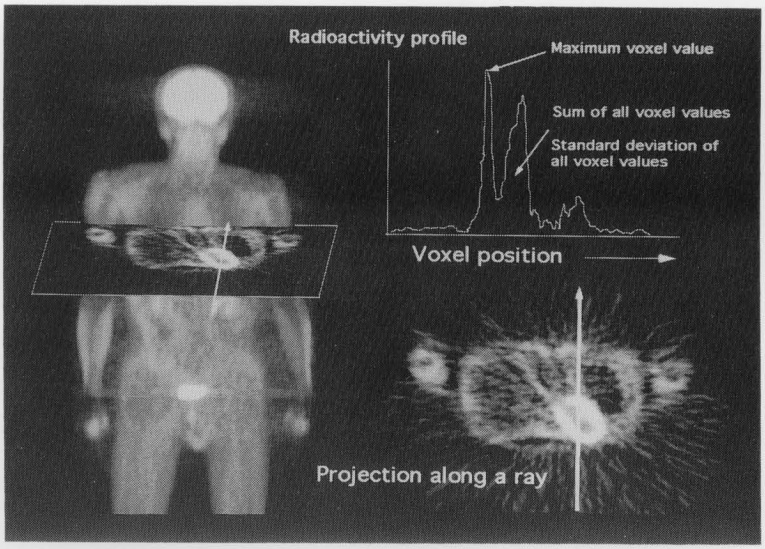

Fig. 1 Production of a projection reformatted image from 3D volume image data. A large number of parallel rays penetrate the whole-body PET volume. The radioactivity profile of each ray will define one pixel in the projection image by a mathematical procedure. In this study, the projection pixel is calculated from the maximum voxel value, the sum of all voxel values and the standard deviation of all voxel values along each projection ray. A two-dimensional projection image is reconstructed by the calculation of all rays.

a radioisotope inside the body. Production of projection reformatted 2D images from 3D volume data has become a popular method for presenting MR and CT angiographic data. Maximum intensity projection (MIP) is a common reconstruction technique used for obtaining 3D images of abdominal vessels from spiral body CT data,[6,7] of intrathoracic masses from MR angiography[8] and of intracranial vessels from brain MR data.[9] However, the projection image used in the whole-body PET image was a planar (rectilinear) image.[10–12]

In this study, we reduced the number of whole-body PET images by calculating the 2D projection image with different algorithms and evaluated the merit of data processing of whole-body PET images for the visualization and detection of tumors.

MATERIALS AND METHODS

Patients

Eight whole-body PET scans with ^{18}F-FDG were obtained in patients referred for tumor staging. The subjects were five women and three men with a mean age of 61 years. None of them suffered from diabetes mellitus. The study protocol was approved by the Ethics Committee for Clinical Research of Tohoku University and all patients gave their written informed consent before their inclusion in the study.

PET study

All data were acquired on a whole-body PET scanner (SET-2400W, Shimadzu, Kyoto, Japan).[13] The scanner consists of four rings of 112 BGO detector units (22.8 mm in-plane × 50 mm axial × 30 mm depth). Each detector unit has a 6 (in-plane) × 8 (axial) array of BGO crystals coupled to two dual photomultiplier tubes. They are arranged in 32 rings giving 63 simultaneous 2D image planes. The axial field-of-view of the scanner is 20 cm. In-plane spatial resolution was 3.9 mm FWHM at the center of the field-of-view, 4.4 mm FWHM tangentially and 5.4 mm FWHM radially at 100 mm from the center. Average axial resolution was 4.5 mm FWHM at the center and 5.8 mm FWHM at a radial position 100 mm from the center.

All patients were asked to refrain from eating and drinking (except for water) for at least 4 hr before scanning. Thirty minutes after an intravenous injection of 185–370 MBq of ^{18}F-FDG, 2D emission scans were obtained for 5 min at each of the contiguous bed positions. Before emission scans, all patients were asked to void. Then scanning was begun at the lower extremity and proceeded towards the patient's head with a minimum amount of activity in the bladder. By acquiring data from overlapping body levels, the effective axial field-of-view was 18.5 cm per bed position, since there is little gain of sensitivity at the edge of the scanner. Six to eight bed positions covered a 111–148 cm total axial field-of-view with 294–392 transaxial images. Post-injection transmission scans were obtained for attenuation correction with a retractable ^{68}Ge rotating rod source.[14]

Image processing and analysis

Two-dimensional images

After reconstructing transverse images using conven-

Table 1 Detection of positive focus by maximum intensity projection (MIP) image, standard deviation projection (SD) image and summed voxel projection (SUM) images compared with original 2D images

Patient no.	Age/Gender	Diagnosis	Number of focus			
			2D	MIP	SD	SUM
1.	59/F	Breast cancer (multiple bone metastases)	28	22	14	9
2.	29/F	Hodgkin's disease	7	7	6	4
3.	70/F	Lung cancer	1	1	1	1
4.	70/F	Uterine cancer (multiple bone metastases)	40	38	33	13
5.	70/M	Malignant lymphoma	3	3	2	0
6.	68/M	Gastric cancer (multiple liver metastases)	15	12	5	4
7.	30/F	Hodgkin's disease	3	3	1	0
8.	64/M	Esophageal cancer (lymph nodes metastases)	5	5	4	4
Total			102	91	66	35
(%)			100	89.2	64.7	34.3

tional filtered back-projection, the series of images were stacked in a three-dimensional volume and linearly interpolated to isotropic voxels (4 mm × 4 mm × 4 mm), allowing for display of whole-body images in the transaxial, sagittal and coronal planes. Localization of ^{18}F-FDG was evaluated by one observer in all studies. The images were visually analyzed on a terminal display of a PET workstation. For image interpretation, the observer was able to adjust window display settings and the image planes and levels independently. A positive focus was defined as a focal area of increased activity relatively higher than that of surrounding tissue excluding physiological accumulations such as brain, heart and bladder.

Projection images

Projection images were reconstructed by using three different algorithms for the evaluation of the activity profiles. The basic idea of the projection reconstruction techniques is shown in Figure 1. Two-dimensional projections were computed by penetrating the entire tomographic volume of a whole-body PET image with many parallel rays. A display pixel's value was calculated as a function of the ray passing through the volume. MIP technique displayed the highest voxel value along a ray projected through the 3D volume data. The display pixel was also calculated as a sum (integral) of all voxel values (SUM) and a standard deviation of all voxel values (SD). The best threshold value was determined visually for each reconstructed image on a terminal display. The observer was also able to adjust window display settings. The reconstruction programs were written in C language on a PET workstation and a projection image was calculated within 5 seconds. Although the reformatted images could be calculated for arbitrary projection angles in the plane of the z-axis or height, only two images (antero-posterior and lateral projection) were used in this study.

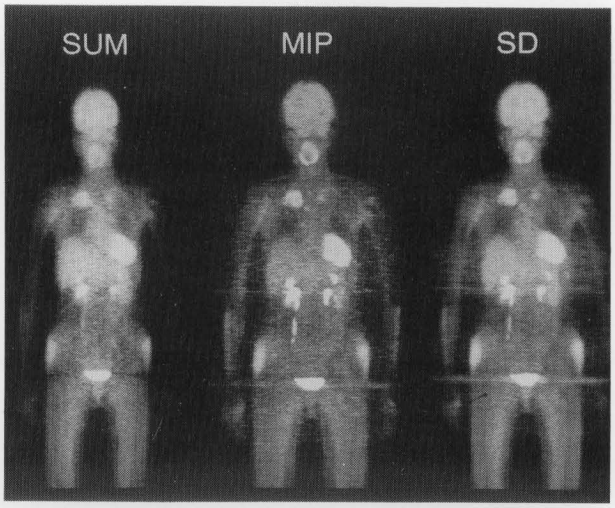

Fig. 2 Whole-body ^{18}F-FDG projection images of a lung cancer patient. The images are based on the maximum voxel value (MIP), the sum of all voxel values (SUM) and the standard deviation of all voxel values (SD) along each antero-posterior projection ray. A tumor in the right upper lobe is shown in all images.

RESULTS

A hundred and two positive sites were found in the original 2D images (Table 1). The percentage of detected sites in projection images of each algorithm was 89.2% (MIP), 64.7% (SD) and 34.3% (SUM), respectively. As shown in Figure 2, when a tumor was large or in the lung, a hot area was clearly visualized in all three projection images. Physiological ^{18}F-FDG accumulations of variable intensity were also observed in brain, heart, renal calices, ureter, bladder and muscle.[15] In the multiple metastatic case of a breast cancer patient, most of the hot

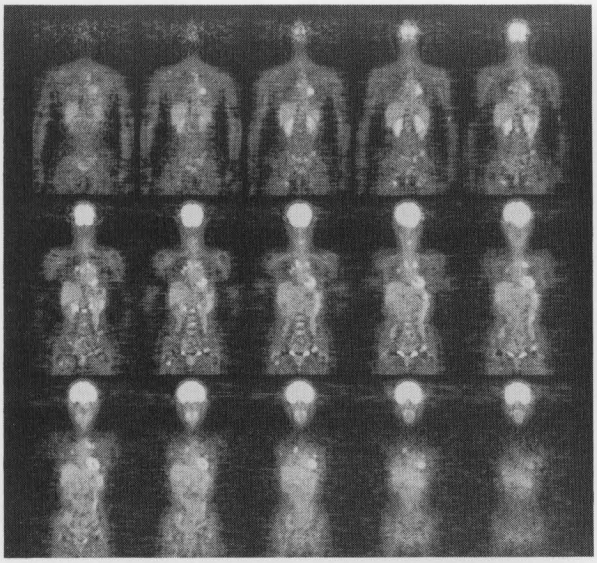

Fig. 3 Coronal whole-body FDG images of a patient with a history of breast cancer show multiple metastases. Every third slice of coronal data set is presented. Projection images are shown in Figure 4.

spots in the original 2D images (Fig. 3) were visualized on MIP reformatted images as shown in Figure 4. The hot spots in the neck and mediastinum are not obvious in the SD image. The SUM image failed to visualize many metastatic lesions.

DISCUSSION

In this study, the reformatted images were obtained with three different algorithms and were compared. As shown in the results, the hot spots in a large number of sequential original 2D images were seen on corresponding two MIP reformatted images. In addition, the distribution of hot spots was easily recognized by viewing MIP reformatted whole-body image. The MIP technique seems to be particularly useful for depicting multiple metastatic lesions in the body.

Apparently the SUM algorithm is inferior to the other algorithms for visualizing hot spots in the original 2D images. Although the SUM image may visualize abnormal uptake in the lung, it fails to visualize small lesions in the neck, mediastinum and abdomen. This algorithm is equivalent to the production of a planar image and has been often used for obtaining whole-body displays of PET images for preliminary assessment of radioisotope distribution.

The SD algorithm with careful thresholding visualized 64.7% of hot spots on the original 2D images. The SD images were found inferior to the corresponding MIP image for showing a contrast of small foci in the neck, mediastinum and abdomen. It was difficult to find the correct value for thresholding in particular for those data

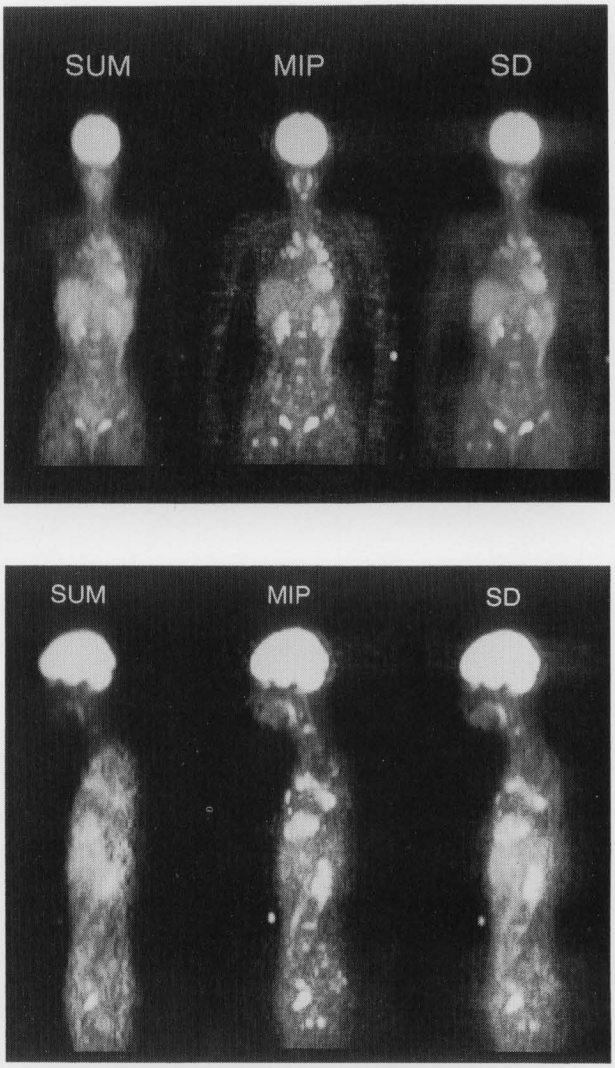

Fig. 4 Whole-body antero-posterior (upper) and lateral (lower) projection images using three algorithms. Most of the hot spots on original 2D images as shown in Figure 3 are visualized on the MIP reformatted image. SD image was somewhat inferior to the corresponding MIP image for showing a contrast of small foci in abdomen. SUM image also failed to visualize the lesions in abdomen.

sets where the activity varied over the volume due to noise in the original 2D images. Proper application of thresholding techniques is necessary to avoid the disappearance of positive foci in the reconstructed images due to incorrect threshold values.

MIP reformatted images are essentially not threshold dependent since the voxel point of highest counts is automatically chosen. The MIP technique has the advantage of operator independence. The other advantage is that the MIP algorithm preserves tissue activity information during image processing. The highest counts in tumor tissue of the original 2D images produce pixel values in positive foci of an MIP image, where the pixel values of

tumor tissue in the reformatted images from other algorithms were not proportional to the tumor counts of the original 2D images. Using the MIP reformatted images from quantitative 2D images with tissue attenuation correction, uptake of a radioisotope into tumor tissue from different studies can be compared quantitatively.

As shown in Table 1, when the number of positive foci increased, we could not detect all of the foci in the MIP images. Because projection reconstruction algorithms do not allow for differentiation between foreground and background, the number of lesions detected in the MIP images seems to be reduced due to superimposition. Nevertheless, even if one hot spot is superimposed over the another hot spot, we can recognize the existence of at least one hot spot and determine the true positions of the hot spots from corresponding transaxial images. To avoid the superimposition of known physiological uptake such as ^{18}F-FDG accumulation into cardiac muscle and bladder, reformatted images of different angles are helpful.

Since the MIP image did not fail to visualize the existence of positive foci, the image can be used for the cancer screening. However, in this study we do not intend to compare the sensitivity of tumor detection with MIP images and original 2D images due to the limited number of patients we studied. At present, MIP images should be interpreted together with the original 2D images. Further knowledge of display properties and artifacts is also necessary for correct interpretation of MIP images.[16]

CONCLUSION

Projection reconstruction algorithms were applied to the whole-body PET images. The initial results suggest the usefulness of an MIP reformatted whole-body image for the easy preliminary assessment of tumor distribution in oncologic PET study.

REFERENCES

1. Larcos G, Maisey MN. FDG-PET screening for cerebral metastases in patients with suspected malignancy. *Nucl Med Commun* 17: 197–198, 1996.
2. Yasuda S, Ide M, Takagi S, Shohtsu A. Cancer screening with whole-body FDG PET. *KAKU IGAKU (Jpn J Nucl Med)* 33: 1065–1071, 1996. (in Japanese)
3. Adler LP, Faulhaber PF, Schnur KC, Al-Kasi NL, Shenk RR. Axillary lymph node metastases: screening with [F-18]2-deoxy-2-fluoro-D-glucose (FDG) PET. *Radiology* 203: 323–327, 1997.
4. Hoh CK, Glaspy J, Rosen P, Dahlbom M, Lee SJ, Kunkel L, et al. Whole-body FDG-PET imaging for staging of Hodgkin's disease and lymphoma. *J Nucl Med* 38: 343–348, 1997.
5. Minoshima S, Frey KA, Koeppe RA, Foster NL, Kuhl DE. A diagnostic approach in Alzheimer's disease using three-dimensional stereotactic surface projections of fluorine-18-FDG PET. *J Nucl Med* 36: 1238–1248, 1995.
6. Winter TC III, Nghiem HV, Freeny PC, Hommeyer SC, Mack LA. Hepatic arterial anatomy: demonstration of normal supply and vascular variants with three-dimensional CT angiography. *Radiographics* 15: 771–780, 1995.
7. Rubin GD, Dake MD, Napel SA, McDonnell CH, Jeffrey RB Jr. Three-dimensional spiral CT angiography of the abdomen: initial clinical experience. *Radiology* 186: 147–152, 1993.
8. Kauczor H-U, Layer G, Schad LR, Müller-Schimpfle M, Tuengerthal SJ, Vogt-Moykopf I, et al. Clinical applications of MR angiography in intrathoracic masses. *J Comput Assist Tomogr* 15: 409–417, 1991.
9. Keller PJ, Drayer BP, Fram EK, Williams KD, Dumoulin CL, Souza SP. MR angiography with two-dimensional acquisition and three-dimensional display. *Radiology* 173: 527–532, 1989.
10. Phelps ME, Hoffman EJ, Huang S-C, Kuhl DE. ECAT: a new computerized tomographic imaging system for positron-emitting radiopharmaceuticals. *J Nucl Med* 19: 635–647, 1978.
11. Guerrero TM, Hoffman EJ, Dahlbom M, Cutler PD, Hawkins RA, Phelps ME. Characterization of a whole body imaging technique for PET. *IEEE Trans Nucl Sci* NS-37: 676–680, 1990.
12. Dahlbom M, Hoffman EJ, Hoh CK, Schiepers C, Rosenqvist G, Hawkins RA, et al. Whole-body positron emission tomography: Part I. Methods and performance characteristics. *J Nucl Med* 33: 1191–1199, 1992.
13. Fujiwara T, Watanuki S, Yamamoto S, Miyake M, Seo S, Itoh M, et al. Performance evaluation of a large axial field-of-view PET scanner: SET-2400W. *Ann Nucl Med* 11: 307–313, 1997.
14. Oda K, Senda M, Toyama H, Ishii K, Amano M. Attenuation correction using postinjection transmission measurements for PET: the optimization of measurement conditions. *KAKU IGAKU (Jpn J Nucl Med)* 31: 37–41, 1994. (in Japanese)
15. Engel H, Steinert H, Buck A, Berthold T, Huch Böni RA, von Schulthess GK. Whole-body PET: physiological and artifactual fluorodeoxyglucose accumulations. *J Nucl Med* 37: 441–446, 1996.
16. Anderson CM, Saloner D, Tsuruda JS, Shapeero LG, Lee RE. Artifacts in maximum-intensity-projection display of MR angiograms. *AJR* 154: 623–629, 1990.